# Renormalized mean-field analysis of antiferromagnetism and d-wave superconductivity in the two-dimensional Hubbard model

J. Reiss[1], D. Rohe[2], and W. Metzner[1]

[1] *Max-Planck-Institute for Solid State Research, D-70569 Stuttgart, Germany*

[2] *Centre de Physique Théorique, Ecole Polytechnique, CNRS-UMR 7644, 91128 Palaiseau Cedex, France*

(Dated: February 6, 2008)

We analyze the competition between antiferromagnetism and superconductivity in the two-dimensional Hubbard model by combining a functional renormalization group flow with a mean-field theory for spontaneous symmetry breaking. Effective interactions are computed by integrating out states above a scale $\Lambda_{\rm MF}$ in one-loop approximation, which captures in particular the generation of an attraction in the d-wave Cooper channel from fluctuations in the particle-hole channel. These effective interactions are then used as an input for a mean-field treatment of the remaining low-energy states, with antiferromagnetism, singlet superconductivity and triplet $\pi$-pairing as the possible order parameters. Antiferromagnetism and superconductivity suppress each other, leaving only a small region in parameter space where both orders can coexist with a sizable order parameter for each. Triplet $\pi$-pairing appears generically in the coexistence region, but its feedback on the other order parameters is very small.

PACS: 71.10.Fd, 74.20.-z, 75.10.-b

## I. INTRODUCTION

Soon after the discovery of high-temperature superconductivity in cuprate compounds, Anderson[1] pointed out that the essential physics of the electrons in the copper-oxide planes of these materials could be described by the two-dimensional Hubbard model. The model describes tight-binding electrons with a local repulsion $U > 0$, as specified by the Hamiltonian

$$H = \sum_{\mathbf{i},\mathbf{j}} \sum_{\sigma} t_{\mathbf{ij}}\, c^{\dagger}_{\mathbf{i}\sigma} c_{\mathbf{j}\sigma} + U \sum_{\mathbf{j}} n_{\mathbf{j}\uparrow} n_{\mathbf{j}\downarrow} \,. \tag{1}$$

in standard second quantization notation. A hopping amplitude $-t$ between nearest neighbors and an amplitude $-t'$ between next-nearest neighbors on a square lattice leads to the dispersion relation $\epsilon_{\mathbf{k}} = -2t\,(\cos k_x + \cos k_y) - 4t' \cos k_x \cos k_y$ for single-particle states.

In agreement with the generic phase diagram of the cuprates, the Hubbard model is an antiferromagnetic insulator at half-filling (provided $t'$ is not too big), and is expected to become a d-wave superconductor away from half-filling in two dimensions already for quite some time.[2] In particular, the exchange of antiferromagnetic spin fluctuations has been proposed as a plausible mechanism leading to d-wave pairing.[3,4,5] It turned out to be very hard to detect superconductivity in the Hubbard model by exact numerical computation,[2,7] as a consequence of finite size and/or temperature limitations.

The tendency toward antiferromagnetism and d-wave pairing in the two-dimensional Hubbard model is present already at weak coupling. However, conventional perturbation theory breaks down in the most interesting density regime, since competing infrared divergences appear as a consequence of Fermi surface nesting and van Hove singularities.[8,9,10] A controlled treatment of these divergences can be achieved by a renormalization group (RG) analysis, which takes into account the particle-particle and particle-hole channels on equal footing.

A suitable framework for a systematic RG analysis of the 2D Hubbard model is provided by the so-called exact or *functional* RG.[11] In this approach, fermionic fields in a functional integral representation of the model are integrated successively by descending step by step in energy scales. This can be formulated as an exact hierarchy of flow equations for the effective interactions. The energy scale of the fields, $\Lambda$, is the flow parameter. Several groups have computed the flow of effective two-particle interactions for the two-dimensional Hubbard model, using various versions of the functional RG in one-loop approximation.[12,13,14,15] Antiferromagnetic and superconducting instabilities were detected from the flow of the corresponding susceptibilities.

At sufficiently low temperatures, and in particular at $T = 0$, the effective two-particle interaction $\Gamma^{\Lambda}$ obtained from a one-loop approximation diverges at a finite scale $\Lambda_c > 0$, that is, before all fields have been integrated out. Hence, one is running into a strong coupling problem in the low-energy limit, even in the case of a weak bare interaction.

If the vertex function diverges only in the Cooper channel, driven by the particle-particle contribution to the flow, the strong coupling problem emerging in the low-energy region can be controlled by exploiting $\Lambda_c$ as a small parameter.[16] The scale $\Lambda_c$ is exponentially small for a small bare interaction. The formation of a superconducting ground state can then be described essentially by a BCS mean-field theory with renormalized input parameters. In the two-dimensional Hubbard model, an instability where the interactions diverge only in the Cooper channel is realized at sufficiently small $U$, if the Fermi surface stays away from van Hove points.[12,13,14,15] At van Hove filling the effective interactions diverge also in other channels even in the weak coupling limit. Although superconductivity then has to compete with other instabilities, the one-loop flow indicates that it is still the leading instability for a moderate $t' \neq 0$ and sufficiently small $U$.[13,14,17]

In principle, spontaneous symmetry breaking can be handled within the functional RG

framework by adding an infinitesimal symmetry breaking term at the beginning of the flow, which is then promoted to a finite order parameter at the scale $\Lambda_c$.[18,19] So far, this approach has been worked out in practice only for mean-field models. Order parameter fluctuations are most conveniently treated by introducing appropriate bosonic fields, as discussed recently for antiferromagnetic order in the half-filled Hubbard model.[20]

In case of competing order parameters, such as antiferromagnetism and d-wave superconductivity, a full RG treatment of spontaneous symmetry breaking and order parameter fluctuations is a rather ambitious long-term goal. In the present work, we explore a simpler alternative and combine the RG with a mean-field (MF) theory of symmetry breaking. In this RG+MF approach the one-loop flow is stopped at a scale $\Lambda_{\rm MF}$ that is small compared to the band width, but still safely above the scale $\Lambda_c$ where the two-particle vertex diverges. At this point the vertex has developed already a pronounced momentum dependence, reflecting in particular antiferromagnetic and superconducting correlations. The integration over the remaining modes, below $\Lambda_{\rm MF}$, is treated in a mean-field approximation allowing, in particular, antiferromagnetic and superconducting order. Low-energy fluctuations are thereby neglected. The mean-field Hamiltonian is defined on a restricted momentum region near the Fermi surface, with $|\epsilon_{\mathbf{k}} - \mu| < \Lambda_{\rm MF}$, and the effective interactions entering the mean-field equations are extracted from $\Gamma^{\Lambda_{\rm MF}}$. A very short account of some RG+MF results has appeared recently in Ref. 21.

Our theory extends previous mean-field treatments of antiferromagnetism and d-wave superconductivity in two-dimensional Hubbard-type and t-J models, where the effective interactions were specified by an ad hoc ansatz or identified with bare microscopic interactions,[22,23,24,25] while we compute the effective interactions by integrating out fluctuations.

In Sec. II we will review the functional RG and the structure of the flow equations for the effective interactions on one-loop level, focussing on the Wick ordered version used in the present work. The mean-field equations for antiferromagnetism and superconductivity, including a possible coexistence of both, will be derived in Sec. III. Results from the combined RG+MF analysis for the 2D Hubbard model will be presented in Sec. IV. In particular, we will analyze which phases are stabilized for various choices of hopping, interaction and density, and we will show results for the size and shape (momentum dependence) of the relevant order parameters. We conclude with a summary of the main results in Sec. V.

## II. RENORMALIZATION GROUP

All versions of the functional RG for interacting Fermi systems are variants of Wilson's[26] momentum shell RG, where fermionic fields are integrated out by descending successively from the modes with highest energy down to the Fermi surface.[27] This type

of RG is also the basis for important rigorous work on two-dimensional Fermi systems.[28] The successive integration of modes can be formulated as an exact hierarchy of flow equations for effective interactions (one-particle, two-particle etc.).[28,29] A similar hierarchy can be obtained by using the interaction strength instead of a cutoff as flow parameter.[30] We focus on the Wick-ordered version of the functional RG, which we will use in our calculations.

### A. Wick ordered flow equations

Before turning to approximations, let us first sketch the structure and derivation of the exact flow equations (for details, see Salmhofer[28] and Ref. 13). The flow parameter $\Lambda$ is introduced as an infrared cutoff for the bare propagator, such that contributions from states with momenta obeying $|\epsilon_{\mathbf{k}} - \mu| < \Lambda$ are suppressed. All Green functions of the interacting system will then depend on $\Lambda$, and the true theory is recovered only in the limit $\Lambda \to 0$. The RG equations are most conveniently obtained from the effective potential $\mathcal{V}^\Lambda$, which is the generating functional for connected Green functions with bare propagators amputated from the external legs. Taking a $\Lambda$-derivative one obtains an exact functional flow equation for this quantity. Expanding $\mathcal{V}^\Lambda$ on both sides of the flow equation in powers of the fermionic fields (i.e. Grassmann variables), and comparing coefficients, one obtains the so-called Polchinski equations[31] for the effective m-body interactions. These equations were used by Zanchi and Schulz[12] in their RG analysis of the two-dimensional Hubbard model. An alternative expansion in terms of Wick ordered monomials of fermion fields yields flow equations for the corresponding m-body interactions $V_m^\Lambda$ with a particularly convenient structure (see Fig. 1).[28] The flow of $V_m^\Lambda$ is given as a bilinear form of other

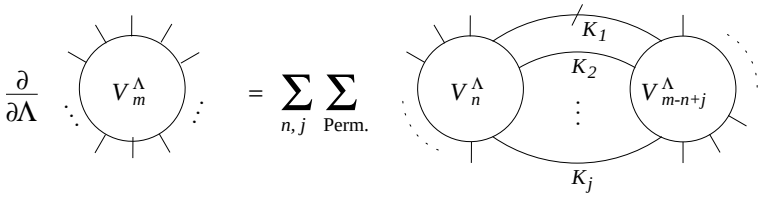


FIG. 1: Diagrammatic representation of the flow equation for $V_m^\Lambda$ in the Wick ordered version of the functional RG. The line with a slash corresponds to $\partial G_0^{<\Lambda}/\partial\Lambda$, the others to $G_0^{<\Lambda}$; all possible pairings leaving $m$ incoming and $m$ outgoing external legs have to be summed.

n-body interactions (at the same scale $\Lambda$), which are connected by lines corresponding to the propagator

$$G_0^{<\Lambda}(k_0, \mathbf{k}) = \frac{\Theta(\Lambda - |\xi_{\mathbf{k}}|)}{ik_0 - \xi_{\mathbf{k}}} \,, \tag{2}$$

where $\xi_{\mathbf{k}} = \epsilon_{\mathbf{k}} - \mu$, and one line corresponding to $\partial_\Lambda G_0^{<\Lambda}(k_0, \mathbf{k})$. Note that the support of $G_0^{<\Lambda}(k_0, \mathbf{k})$ is restricted to momenta with $|\xi_{\mathbf{k}}|$ *below* the scale $\Lambda$. These soft mode

propagators come into play via the Wick ordering, which is given by (scale dependent) contractions with $G_0^{<\Lambda}(k_0, \mathbf{k})$. For $\Lambda \to 0$, the effective interactions remain unaffected by the Wick ordering, since $G_0^{<\Lambda}(k)$ vanishes in that limit. For small $\Lambda$, the momentum integrals on the right hand side of the flow equation are restricted to momenta close to the Fermi surface (see Fig. 2).

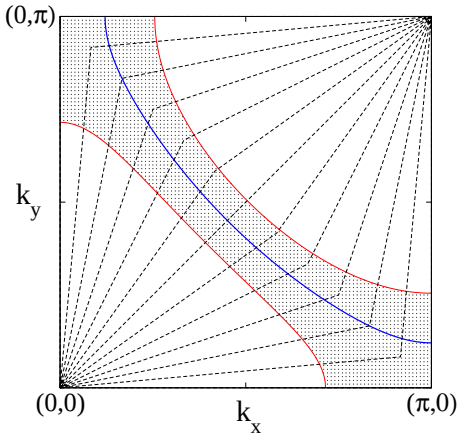


FIG. 2: (Color online) A typical Fermi surface (bold line) and the support of the propagator $G_0^{<\Lambda}(k_0, \mathbf{k})$ (dotted region) in the first quadrant of the Brillouin zone. The dashed lines mark the boundaries of the "patches" used for the discretization of the momentum dependence of the effective two-particle interaction.

With the initial condition $\mathcal{V}^{\Lambda_0} =$ bare interaction, where $\Lambda_0 = \max|\xi_{\mathbf{k}}|$, the above flow equations determine the exact flow of the effective interactions as $\Lambda$ sweeps over the entire energy range from the band edges down to the Fermi level. Since the Wick ordered flow below scale $\Lambda$ involves only low-energy states with $|\xi_{\mathbf{k}}| < \Lambda$, it yields a continuous sequence of effective low-energy models with effective interactions acting on a restricted momentum space.

### B. One-loop flow

To detect instabilities of the system in the weak-coupling limit, it is sufficient to truncate the infinite hierarchy of flow equations described by Fig. 1 at second order in the effective two-particle interaction $V_2^\Lambda$. Contributions to the flow of $V_2^\Lambda$ involving effective three-particle interactions and higher $m$-body terms are at least of third order in $V_2^\Lambda$. The leading contribution from the effective one-particle interaction $V_1^\Lambda$ can be absorbed by a simple shift of the chemical potential. The remaining influence of $V_1^\Lambda$ on the flow of $V_2^\Lambda$ is of third order an can thus be neglected.

The flow of the effective two-particle interaction $V_2^\Lambda$ is thus given by one-loop terms involving only $V_2^\Lambda$, and no other $m$-body terms. In the following, we write $\Gamma^\Lambda$ instead of

$V_2^\Lambda$ for the two-particle interaction. Putting arrows on the lines to distinguish creation and annihilation operators, one obtains the diagrammatic representation of the flow equation shown in Fig. 3. To write the momentum, energy and spin dependences of $\Gamma^\Lambda$, we collect

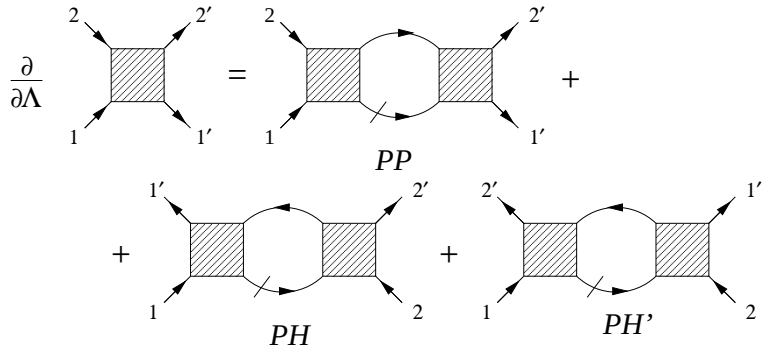


FIG. 3: Flow equation for the effective two-particle interaction $\Gamma^\Lambda$ in one-loop approximation with the particle-particle channel (PP) and the two particle-hole channels (PH and PH').

$k = (k_0, \mathbf{k})$ and $\sigma$ in a single variable $K$. In $\Gamma^\Lambda(K_1', K_2'; K_1, K_2)$, the variables $K_1$ and $K_2$ refer to incoming, the variables $K_1'$ and $K_2'$ to outgoing particles. With this notation, the explicit one-loop flow equation for $\Gamma^\Lambda$ reads[13]

$$\begin{aligned}\frac{\partial}{\partial\Lambda}\Gamma^\Lambda(K_1', K_2'; K_1, K_2) = \\ \frac{1}{\beta L}\sum_{K,K'} \frac{\partial}{\partial\Lambda}\left[G_0^{<\Lambda}(K)\, G_0^{<\Lambda}(K')\right] \\ \times\Big[\frac{1}{2}\Gamma^\Lambda(K_1', K_2'; K, K')\,\Gamma^\Lambda(K, K'; K_1, K_2) \\ - \Gamma^\Lambda(K_1', K; K_1, K')\,\Gamma^\Lambda(K', K_2'; K, K_2) \\ + \Gamma^\Lambda(K_2', K; K_1, K')\,\Gamma^\Lambda(K', K_1'; K, K_2)\Big]\,,\end{aligned} \tag{3}$$

where $L$ is the number of lattice sites, and $\beta$ the inverse temperature. The three terms on the right hand side are the contributions from the particle-particle channel (PP) and the two particle-hole channels (PH and PH'). For translation invariant systems momentum conservation implies that $\Gamma^\Lambda(K_1', K_2'; K_1, K_2) \neq 0$ only if $k_1 + k_2 = k_1' + k_2'$, so that the sum over $k$ and $k'$ in (3) is reduced to a single energy-momentum sum.

For a spin-rotation invariant system the spin structure of the two-particle interaction can be written as

$$\Gamma^\Lambda(K_1', K_2'; K_1, K_2) = \Gamma_s^\Lambda(k_1', k_2'; k_1, k_2)\, S_{\sigma_1',\sigma_2';\sigma_1,\sigma_2} + \Gamma_t^\Lambda(k_1', k_2'; k_1, k_2)\, T_{\sigma_1',\sigma_2';\sigma_1,\sigma_2}\,, \tag{4}$$

where

$$\begin{aligned} S_{\sigma_1',\sigma_2';\sigma_1,\sigma_2} &= \tfrac{1}{2}\left(\delta_{\sigma_1\sigma_1'}\delta_{\sigma_2\sigma_2'} - \delta_{\sigma_1\sigma_2'}\delta_{\sigma_2\sigma_1'}\right) \\ T_{\sigma_1',\sigma_2';\sigma_1,\sigma_2} &= \tfrac{1}{2}\left(\delta_{\sigma_1\sigma_1'}\delta_{\sigma_2\sigma_2'} + \delta_{\sigma_1\sigma_2'}\delta_{\sigma_2\sigma_1'}\right) \end{aligned} \tag{5}$$

are the projection operators on singlet and triplet states in a two-particle spin space, respectively. The antisymmetry of $\Gamma^\Lambda$ with respect to $K_1 \leftrightarrow K_2$ or $K_1' \leftrightarrow K_2'$ implies that $\Gamma_s^\Lambda$ is symmetric and $\Gamma_t^\Lambda$ antisymmetric under exchange of the variables $k_1$ and $k_2$ or $k_1'$ and $k_2'$. Inserting the above decomposition in singlet and triplet terms, the spin sums can be easily carried out and one obtains a coupled set of equations for $\Gamma_s^\Lambda$ and $\Gamma_t^\Lambda$.

It is clearly impossible to solve the flow equations with the full energy and momentum dependence of the two-particle interaction, since $\Gamma^\Lambda$ has three independent energy and momentum variables. The problem can however be simplified by ignoring dependences which are *irrelevant* (in the RG sense) in the low energy limit, namely the energy dependence and the momentum dependence normal to the Fermi surface.[27] Hence, we compute the flow of the two-particle interaction at zero energy and with at least three momenta on the Fermi surface (the fourth being determined by momentum conservation). On the right hand side of the flow equation we approximate the interaction by its zero energy value with three momenta projected on the Fermi surface (if not already there). Note that this projection procedure is exact for the initial two-particle interaction, since the Hubbard interaction is momentum and energy independent. The remaining tangential momentum dependence is discretized. The momentum-dependence of the two-particle vertex is thus approximated by a step function which is constant on "patches" (sectors) in the Brillouin zone.[12,13,14] Here we use patches defined by straight lines connecting the points $(0,0)$ and $(\pi,\pi)$ to the magnetic Brillouin zone boundary (also known as "umklapp surface"), see Fig. 2.

Neglecting the energy dependence of $\Gamma^\Lambda$, the Matsubara sum in the flow equation can be done analytically. Due to the sharp momentum cutoff the momentum integral can be easily reduced to a one-dimensional integral. The latter, and the integration of the flow, has to be performed numerically.

We will stop the flow at a scale $\Lambda_{\rm MF}$ well above the scale $\Lambda_c$ at which $\Gamma^\Lambda$ diverges. The remaining degrees of freedom will be treated in a mean-field approximation to be described in the next section. The output of the flow, $\Gamma^{\Lambda_{\rm MF}}$, is the input interaction for the mean-field theory.

## III. MEAN-FIELD THEORY

The divergence of the effective two-particle interaction $\Gamma^\Lambda$ as a function of decreasing $\Lambda$ signals an instability leading to an ordered phase via spontaneous symmetry breaking.[32] The simplest way to treat spontaneous symmetry breaking is provided by a mean-field approximation. For a specific type of order, only interactions with a very restricted choice of momenta are picked up by the mean-field theory. For example, in the BCS mean-field theory of superconductivity, the only relevant interaction processes involve particles with vanishing total momentum ($\mathbf{k}_1 + \mathbf{k}_2 = 0$). Vice versa, in the thermodynamic limit the

mean-field approximation provides the exact solution of a *reduced* Hamiltonian, in which the interaction is restricted to the relevant momenta from the beginning.

### A. Reduced Hamiltonian

Here we specify our reduced Hamiltonian, and link the interaction terms to the effective two-particle interaction obtained from the RG. In addition to interactions driving antiferromagnetism and superconductivity, we will also include several other interaction terms, since they do not lead to major complications, make the general structure of the theory more transparent, and may be useful for a more general analysis in the future.

The reduced Hamiltonian has the form

$$H^{\rm red} = H_0 + H_{\rm I}^{\rm red} \ , \tag{6}$$

where $H_0 = \sum_{\mathbf{k},\sigma} \epsilon_{\mathbf{k}} \, n_{\mathbf{k}\sigma}$ is the kinetic energy and $H_{\rm I}^{\rm red}$ the reduced interaction. The latter contains four terms,

$$H_{\rm I}^{\rm red} = H_{\rm I}^{n,0} + H_{\rm I}^{n,\pi} + H_{\rm I}^{p,0} + H_{\rm I}^{p,\pi} \ , \tag{7}$$

which we now specify one by one.

The first term is a density-density interaction with zero momentum transfer (forward scattering),

$$H_{\rm I}^{n,0} = \frac{1}{2L} \sum_{\mathbf{k},\mathbf{k}'} \sum_{\sigma,\sigma'} F_{\mathbf{k}\mathbf{k}'}^{\sigma\sigma'} \, n_{\mathbf{k}\sigma} \, n_{\mathbf{k}'\sigma'} \ . \tag{8}$$

This term captures Fermi liquid interaction effects, and can lead to charge or spin density instabilities such as phase separation, ferromagnetism, or a d-wave Pomeranchuk instability[17,33].

The second term is a density-density interaction with momentum transfer $\mathbf{Q} = (\pi, \pi)$,

$$H_{\rm I}^{n,\pi} = \frac{1}{2L} \sum_{\mathbf{k},\mathbf{k}'} \sum_{\sigma,\sigma'} U_{\mathbf{k}\mathbf{k}'}^{\sigma\sigma'} \, n_{\mathbf{k}\sigma}^{\pi} \, n_{\mathbf{k}'\sigma'}^{\pi} \ , \tag{9}$$

with $n_{\mathbf{k}\sigma}^{\pi} = a_{\mathbf{k}\sigma}^{\dagger} a_{\mathbf{k}+\mathbf{Q},\sigma}$. Note that $\mathbf{k}+\mathbf{Q} = \mathbf{k}-\mathbf{Q}$. This term drives charge or spin density wave instabilities with a wave vector $\mathbf{Q}$ and arbitrary form factors (s-wave, d-wave etc.), including, in particular, antiferromagnetic order.

The third term is a singlet pairing interaction between particles with total momentum zero (Cooper channel),

$$H_{\rm I}^{p,0} = \frac{1}{L} \sum_{\mathbf{k},\mathbf{k}'} V_{\mathbf{k}\mathbf{k}'} \, p_{\mathbf{k}}^{\dagger} \, p_{\mathbf{k}'} \ , \tag{10}$$

with $p_{\mathbf{k}} = a_{-\mathbf{k}\downarrow} a_{\mathbf{k}\uparrow}$ and $p_{\mathbf{k}}^{\dagger}$ its hermitian conjugate. There is no factor 1/2 here, since spin variables are fixed. This term drives spin-singlet superconductivity.

Finally, we include a triplet pairing interaction between particles with a total momentum $\mathbf{Q}$,

$$H_{\mathrm{I}}^{p,\pi} = \frac{1}{L}\sum_{\mathbf{k},\mathbf{k}'} V_{\mathbf{k}\mathbf{k}'}^{\pi}\, p_{\mathbf{k}}^{\pi\,\dagger}\, p_{\mathbf{k}'}^{\pi}\ , \tag{11}$$

with $p_{\mathbf{k}}^{\pi} = a_{\mathbf{Q}-\mathbf{k},\downarrow} a_{\mathbf{k}\uparrow}$ and $p_{\mathbf{k}}^{\pi\,\dagger}$ its hermitian conjugate. In case of coexistence of antiferromagnetism and superconducitivity, this term leads to a condensate of pairs with total momentum $\mathbf{Q}$.[23,24,34]

We use the mean-field theory as an approximate treatment of the fermionic degrees of freedom below the energy scale $\Lambda_{\mathrm{MF}}$. Hence, all momenta in the above terms are restricted to a shell around the Fermi surface given by $|\epsilon_{\mathbf{k}} - \mu| < \Lambda_{\mathrm{MF}}$. For the dispersion relation $\epsilon_{\mathbf{k}}$ in $H_0$, we simply use the bare one, that is, we do not keep track of self-energy contributions which may renormalize $\epsilon_{\mathbf{k}}$. Self-energy corrections beyond those which can be absorbed in a shift of $\mu$ appear only at second order in the interactions, and may therefore be neglected at weak coupling.

The coupling functions in $H_{\mathrm{I}}^{\mathrm{red}}$ are extracted from the effective two-particle interaction $\Gamma^{\Lambda_{\mathrm{MF}}}$. Denoting the static (frequency independent) two-particle interaction with generic momenta by $\Gamma^{\Lambda_{\mathrm{MF}}}(\mathbf{k}_1'\sigma_1', \mathbf{k}_2'\sigma_2'; \mathbf{k}_1\sigma_1, \mathbf{k}_2\sigma_2)$, we have

$$F_{\mathbf{k}\mathbf{k}'}^{\sigma\sigma'} \;=\; \frac{1}{2}\,\Gamma^{\Lambda_{\mathrm{MF}}}(\mathbf{k}\sigma, \mathbf{k}'\sigma'; \mathbf{k}\sigma, \mathbf{k}'\sigma')\ , \tag{12}$$

$$U_{\mathbf{k}\mathbf{k}'}^{\sigma\sigma'} \;=\; \frac{1}{2}\,\Gamma^{\Lambda_{\mathrm{MF}}}(\mathbf{k}\sigma, \mathbf{k}'\sigma'; \mathbf{k}+\mathbf{Q}\,\sigma, \mathbf{k}'-\mathbf{Q}\,\sigma')\ , \tag{13}$$

$$V_{\mathbf{k}\mathbf{k}'} \;=\; \frac{1}{2}\,\Gamma_{s}^{\Lambda_{\mathrm{MF}}}(\mathbf{k}, -\mathbf{k}; \mathbf{k}', -\mathbf{k}')\ , \tag{14}$$

$$V_{\mathbf{k}\mathbf{k}'}^{\pi} \;=\; \frac{1}{2}\,\Gamma_{t}^{\Lambda_{\mathrm{MF}}}(\mathbf{k}, \mathbf{Q}-\mathbf{k}; \mathbf{k}', \mathbf{Q}-\mathbf{k}')\ . \tag{15}$$

All these coupling functions are real-valued. Note that there is an overlap between the different coupling functions above for special choices of momenta. For example, for $\mathbf{k}_1 = \mathbf{k}_1' = -\mathbf{k}_2 = -\mathbf{k}_2'$ the vertex belongs to the Cooper and forward scattering channels simultaneously. However, these special momentum sets have zero measure in the thermodynamic limit.

### B. Mean-field decoupling

The mean-field theory involves the following mean fields

$$D_{\mathbf{k}\sigma} = \frac{1}{L}\sum_{\mathbf{k}'\sigma'} F^{\sigma\sigma'}_{\mathbf{k}\mathbf{k}'} \langle n_{\mathbf{k}'\sigma'}\rangle \tag{16}$$

$$D^{\pi}_{\mathbf{k}\sigma} = \frac{1}{L}\sum_{\mathbf{k}'\sigma'} U^{\sigma\sigma'}_{\mathbf{k}\mathbf{k}'} \langle n^{\pi}_{\mathbf{k}'\sigma'}\rangle \tag{17}$$

$$\Delta_{\mathbf{k}} = \frac{1}{L}\sum_{\mathbf{k}'} V_{\mathbf{k}\mathbf{k}'} \langle p_{\mathbf{k}'}\rangle \tag{18}$$

$$\Delta^{\pi}_{\mathbf{k}} = \frac{1}{L}\sum_{\mathbf{k}'} V^{\pi}_{\mathbf{k}\mathbf{k}'} \langle p^{\pi}_{\mathbf{k}'}\rangle \ . \tag{19}$$

The density field $D_{\mathbf{k}\sigma}$ is real. The density field $D^{\pi}_{\mathbf{k}\sigma}$ can be complex and obeys the relation $D^{\pi}_{\mathbf{k}+\mathbf{Q},\sigma} = D^{\pi *}_{\mathbf{k}\sigma}$, which follows directly from $\langle n^{\pi}_{\mathbf{k}+\mathbf{Q},\sigma}\rangle = \langle n^{\pi}_{\mathbf{k}\sigma}\rangle^*$ and $U^{\sigma\sigma'}_{\mathbf{k}+\mathbf{Q},\mathbf{k}'+\mathbf{Q}} = U^{\sigma\sigma'}_{\mathbf{k}\mathbf{k}'}$ . The pairing fields $\Delta_{\mathbf{k}}$ and $\Delta^{\pi}_{\mathbf{k}}$ are generally complex.

The operator products in the interaction terms have the form $b'b$, where $b$ and $b'$ are products of two elementary Fermi operators. In the mean-field decoupling, one approximates $b'b \approx \langle b'\rangle\, b + \langle b\rangle\, b' - \langle b'\rangle\,\langle b\rangle$. The fluctuation term $(b' - \langle b'\rangle)\,(b - \langle b\rangle)$ is thereby neglected. This yields

$$H^{n,0}_{\mathrm{I}} \approx \sum_{\mathbf{k},\sigma} D_{\mathbf{k}\sigma}\, n_{\mathbf{k}\sigma} - \frac{1}{2}\sum_{\mathbf{k},\sigma} D_{\mathbf{k}\sigma}\langle n_{\mathbf{k}\sigma}\rangle \ , \tag{20}$$

$$H^{n,\pi}_{\mathrm{I}} \approx \sum_{\mathbf{k},\sigma} D^{\pi}_{\mathbf{k}\sigma}\, n^{\pi}_{\mathbf{k}\sigma} - \frac{1}{2}\sum_{\mathbf{k},\sigma} D^{\pi}_{\mathbf{k}\sigma}\langle n^{\pi}_{\mathbf{k}\sigma}\rangle \ , \tag{21}$$

$$H^{p,0}_{\mathrm{I}} \approx \sum_{\mathbf{k}} \Delta^*_{\mathbf{k}}\, p_{\mathbf{k}} + \sum_{\mathbf{k}} \Delta_{\mathbf{k}}\, p^{\dagger}_{\mathbf{k}} - \sum_{\mathbf{k}} \Delta^*_{\mathbf{k}}\,\langle p_{\mathbf{k}}\rangle \ , \tag{22}$$

$$H^{p,\pi}_{\mathrm{I}} \approx \sum_{\mathbf{k}} \Delta^{\pi *}_{\mathbf{k}}\, p^{\pi}_{\mathbf{k}} + \sum_{\mathbf{k}} \Delta^{\pi}_{\mathbf{k}}\, p^{\pi\,\dagger}_{\mathbf{k}} - \sum_{\mathbf{k}} \Delta^{\pi *}_{\mathbf{k}}\,\langle p^{\pi}_{\mathbf{k}}\rangle \ . \tag{23}$$

For the above reduced interactions this approximation is exact in the thermodynamic limit. This can be seen quite easily by estimating the size of Feynman diagrams with a reduced interaction or, alternatively, by using a Hubbard Stratonovich decoupling in a functional integral representation.[35]

The Hamiltonian is now quadratic in the fermions and can therefore be diagonalized. We define $K^{\mathrm{MF}} = H^{\mathrm{MF}} - \mu N$, where $H^{\mathrm{MF}}$ is the reduced Hamiltonian in mean-field approximation, and $N = \sum_{\mathbf{k},\sigma} n_{\mathbf{k}\sigma}$ is the total particle number operator. Introducing the Nambu spinor

$$\mathbf{a}_{\mathbf{k}} = (a_{\mathbf{k}\uparrow}, a^{\dagger}_{-\mathbf{k}\downarrow}, a_{\mathbf{k}+\mathbf{Q},\uparrow}, a^{\dagger}_{-\mathbf{k}-\mathbf{Q},\downarrow}) \ , \tag{24}$$

the mean-field Hamiltonian can be written as

$$K^{\mathrm{MF}} = \sum_{\mathbf{k}} \mathbf{a}_{\mathbf{k}}^{\dagger} \mathcal{M}_{\mathbf{k}} \, \mathbf{a}_{\mathbf{k}} + K^{c} \, , \tag{25}$$

where $K^c$ collects all c-number terms, that is, terms without operators, and the quadratic form with the matrix $\mathcal{M}_{\mathbf{k}}$ all quadratic terms. Here the momentum sum extends only over momenta in the *magnetic* Brillouin zone. The matrix $\mathcal{M}_{\mathbf{k}}$ is given by

$$\mathcal{M}_{\mathbf{k}} = \begin{pmatrix} \xi_{\mathbf{k}} + D_{\mathbf{k}\uparrow} & \Delta_{\mathbf{k}} & D^{\pi}_{\mathbf{k}\uparrow} & \Delta^{\pi}_{\mathbf{k}} \\ \Delta^{*}_{\mathbf{k}} & -\xi_{-\mathbf{k}} - D_{-\mathbf{k}\downarrow} & \Delta^{\pi *}_{\mathbf{k}+\mathbf{Q}} & -D^{\pi}_{-\mathbf{k}-\mathbf{Q},\downarrow} \\ D^{\pi}_{\mathbf{k}+\mathbf{Q},\uparrow} & \Delta^{\pi}_{\mathbf{k}+\mathbf{Q}} & \xi_{\mathbf{k}+\mathbf{Q}} + D_{\mathbf{k}+\mathbf{Q},\uparrow} & \Delta_{\mathbf{k}+\mathbf{Q}} \\ \Delta^{\pi *}_{\mathbf{k}} & -D^{\pi}_{-\mathbf{k}\downarrow} & \Delta^{*}_{\mathbf{k}+\mathbf{Q}} & -\xi_{-\mathbf{k}-\mathbf{Q}} - D_{-\mathbf{k}-\mathbf{Q},\downarrow} \end{pmatrix} . \tag{26}$$

Note that $\mathcal{M}_{\mathbf{k}}$ is hermitean since $D^{\pi}_{\mathbf{k}+\mathbf{Q},\sigma} = D^{\pi *}_{\mathbf{k}\sigma}$. The momenta of the mean fields in $\mathcal{M}_{\mathbf{k}}$ are restricted by the cutoff: $D_{\mathbf{k}\sigma}$ and $\Delta_{\mathbf{k}}$ are restricted by the condition $|\xi_{\mathbf{k}}| < \Lambda_{\mathrm{MF}}$, while $D^{\pi}_{\mathbf{k}}$ and $\Delta^{\pi}_{\mathbf{k}}$ contribute only if the two conditions $|\xi_{\mathbf{k}}| < \Lambda_{\mathrm{MF}}$ and $|\xi_{\mathbf{k}+\mathbf{Q}}| < \Lambda_{\mathrm{MF}}$ are satisfied simultaneously. The matrix $\mathcal{M}_{\mathbf{k}}$ has a $2 \times 2$ block structure

$$\mathcal{M}_{\mathbf{k}} = \begin{pmatrix} \mathcal{M}^{0}_{\mathbf{k}} & \mathcal{M}^{\pi}_{\mathbf{k}} \\ \mathcal{M}^{\pi}_{\mathbf{k}+\mathbf{Q}} & \mathcal{M}^{0}_{\mathbf{k}+\mathbf{Q}} \end{pmatrix} , \tag{27}$$

where $\mathcal{M}^{0}_{\mathbf{k}}$ and $\mathcal{M}^{\pi}_{\mathbf{k}}$ are $2 \times 2$ matrices.

The c-number term, $K^c$ contains a contribution from commutators, $\sum_{\mathbf{k}}(\xi_{\mathbf{k}} + D_{\mathbf{k}\downarrow})$, in addition to the c-number terms originating from the mean-field decoupling of the interaction terms.

The matrix $\mathcal{M}_{\mathbf{k}}$ can be diagonalized by a unitary transformation $\mathcal{U}_{\mathbf{k}}$:

$$\sum_{\mathbf{k}} \mathbf{a}_{\mathbf{k}}^{\dagger} \mathcal{M}_{\mathbf{k}} \, \mathbf{a}_{\mathbf{k}} = \sum_{\mathbf{k}} \tilde{\mathbf{a}}_{\mathbf{k}}^{\dagger} \tilde{\mathcal{M}}_{\mathbf{k}} \, \tilde{\mathbf{a}}_{\mathbf{k}} \, , \tag{28}$$

where $\tilde{\mathbf{a}}_{\mathbf{k}} = \mathcal{U}_{\mathbf{k}} \, \mathbf{a}_{\mathbf{k}}$, $\tilde{\mathbf{a}}_{\mathbf{k}}^{\dagger} = \mathbf{a}_{\mathbf{k}}^{\dagger} \mathcal{U}_{\mathbf{k}}^{\dagger}$, and $\tilde{\mathcal{M}}_{\mathbf{k}} = \mathcal{U}_{\mathbf{k}} \, \mathcal{M}_{\mathbf{k}} \, \mathcal{U}_{\mathbf{k}}^{\dagger}$ is a diagonal matrix

$$\tilde{\mathcal{M}}_{\mathbf{k}} = \mathrm{diag}(E^{1}_{\mathbf{k}}, E^{2}_{\mathbf{k}}, E^{3}_{\mathbf{k}}, E^{4}_{\mathbf{k}}) \tag{29}$$

with the eigenvalues $E^{\lambda}_{\mathbf{k}}$, $\lambda = 1, 2, 3, 4$, as entries. The transformed creation and annihilation operators obey fermionic anticommutation relations, $\{\tilde{a}^{\lambda}_{\mathbf{k}}, \tilde{a}^{\lambda' \dagger}_{\mathbf{k}'}\} = \delta_{\lambda\lambda'} \, \delta_{\mathbf{k}\mathbf{k}'}$ , since $\mathcal{U}_{\mathbf{k}}$ is unitary. The block structure (27) implies that the matrices $\mathcal{M}_{\mathbf{k}}$ and $\mathcal{M}_{\mathbf{k}+\mathbf{Q}}$ have the same eigenvalues, which can thus be labelled such that $E^{\lambda}_{\mathbf{k}+\mathbf{Q}} = E^{\lambda}_{\mathbf{k}}$.

### C. General gap equations

The selfconsistency or gap equations can be derived by minimizing the grand canonical potential

$$\Omega = K^{c} - T \sum_{\mathbf{k},\lambda} \ln\left(1 + e^{-\beta \, E^{\lambda}_{\mathbf{k}}}\right) \tag{30}$$

with respect to the expectation values $\langle n_{\mathbf{k}\sigma}\rangle$, $\langle n^\pi_{\mathbf{k}\sigma}\rangle$, $\langle p_{\mathbf{k}}\rangle$, $\langle p^\pi_{\mathbf{k}}\rangle$, or complex conjugates. As shown in Appendix A, the gap equations can be expressed in terms of minors of the matrices

$$\mathcal{M}^\lambda_{\mathbf{k}} = \mathcal{M}_{\mathbf{k}} - E^\lambda_{\mathbf{k}}\mathbf{1} \; . \tag{31}$$

The minor $\det(M^{\lambda,jj'}_{\mathbf{k}})$ is the determinant of the matrix obtained from $\mathcal{M}^\lambda_{\mathbf{k}}$ by deleting the $j$-th row and the $j'$-th column. Minimizing with respect to $\langle n_{\mathbf{k}\sigma}\rangle$ yields

$$D_{\mathbf{k}\sigma} = \frac{1}{L}\sum_{\mathbf{k}'}\sum_\lambda \frac{F^{\sigma\uparrow}_{\mathbf{k}\mathbf{k}'}\det\big(M^{\lambda,11}_{\mathbf{k}'}\big) - F^{\sigma\downarrow}_{\mathbf{k},-\mathbf{k}'}\det\big(M^{\lambda,22}_{\mathbf{k}'}\big)}{\sum_l \det\big(M^{\lambda,ll}_{\mathbf{k}'}\big)}\, f(E^\lambda_{\mathbf{k}'}) + \frac{1}{L}\sum_{\mathbf{k}'} F^{\sigma\downarrow}_{\mathbf{k}\mathbf{k}'} \; , \tag{32}$$

where $f$ is the Fermi function. The last term in (32) stems from the contribution $\sum_{\mathbf{k}} D_{\mathbf{k}\downarrow}$ to $K^c$ mentioned above. Minimizing with respect to $\langle n^\pi_{\mathbf{k}\sigma}\rangle$ yields

$$D^\pi_{\mathbf{k}\sigma} = \frac{1}{L}\sum_{\mathbf{k}'}\sum_\lambda \frac{U^{\sigma\uparrow}_{\mathbf{k}\mathbf{k}'}\det\big(M^{\lambda,13}_{\mathbf{k}'}\big) - U^{\sigma\downarrow}_{\mathbf{k},-\mathbf{k}'}\det\big(M^{\lambda,42}_{\mathbf{k}'}\big)}{\sum_l \det\big(M^{\lambda,ll}_{\mathbf{k}'}\big)}\, f(E^\lambda_{\mathbf{k}'}) \; . \tag{33}$$

Minimization with respect to $\langle p_{\mathbf{k}}\rangle^*$ yields

$$\Delta_{\mathbf{k}} = -\frac{1}{L}\sum_{\mathbf{k}'} V_{\mathbf{k}\mathbf{k}'}\sum_\lambda \frac{\det\big(M^{\lambda,21}_{\mathbf{k}'}\big)}{\sum_l \det\big(M^{\lambda,ll}_{\mathbf{k}'}\big)}\, f(E^\lambda_{\mathbf{k}'}) \; , \tag{34}$$

while minimizing with respect to $\langle p_{\mathbf{k}}\rangle$ would just yield the complex conjugate of the above equation. Minimization with respect to $\langle p^\pi_{\mathbf{k}}\rangle^*$ yields

$$\Delta^\pi_{\mathbf{k}} = -\frac{1}{L}\sum_{\mathbf{k}'} V^\pi_{\mathbf{k}\mathbf{k}'}\sum_\lambda \frac{\det\big(M^{\lambda,41}_{\mathbf{k}'}\big)}{\sum_l \det\big(M^{\lambda,ll}_{\mathbf{k}'}\big)}\, f(E^\lambda_{\mathbf{k}'}) \; , \tag{35}$$

and minimization with respect to $\langle p^\pi_{\mathbf{k}}\rangle$ again the complex conjugate. Note that the momentum sums in the above gap equations extend over the full (not just magnetic) Brillouin zone within the limits imposed by the cutoff.

The denominator in the gap equations can be expressed in terms of the eigenvalues as (see Appendix A)

$$\sum_l \det\big(M^{\lambda,ll}_{\mathbf{k}}\big) = \prod_{\lambda'\neq\lambda}(E^{\lambda'}_{\mathbf{k}} - E^\lambda_{\mathbf{k}}) \; . \tag{36}$$

The electron density $n = -L^{-1}\partial\Omega/\partial\mu$ can be written as

$$n = 1 + \frac{1}{L}\sum_{\mathbf{k}'}\sum_\lambda \frac{\det\big(M^{\lambda,11}_{\mathbf{k}'}\big) - \det\big(M^{\lambda,22}_{\mathbf{k}'}\big)}{\sum_l \det\big(M^{\lambda,ll}_{\mathbf{k}'}\big)}\, f(E^\lambda_{\mathbf{k}'}) \; . \tag{37}$$

The derivation of this relation is almost identical to the one of the gap equation for $D_{\mathbf{k}\sigma}$.

For a numerical evaluation it is sometimes convenient to rewrite the ratios of determinants in the above expressions in terms of the eigenvectors of $\mathcal{M}_{\mathbf{k}}$.[36]

### D. Gap equations for antiferromagnetism and superconductivity

We are mainly interested in the interplay of antiferromagnetism and superconductivity in the two-dimensional Hubbard model. In the numerical solution of the mean-field equations we will therefore ignore $D_{\mathbf{k}\sigma}$. Furthermore, we will restrict $D^{\pi}_{\mathbf{k}\sigma}$ to the spin density wave channel, that is, $D^{\pi}_{\mathbf{k}\uparrow} = -D^{\pi}_{\mathbf{k}\downarrow} \equiv A_{\mathbf{k}}$. The mean-field $A_{\mathbf{k}}$ is related to the staggered magnetisation $m_{\mathbf{k}} = n^{\pi}_{\mathbf{k}\uparrow} - n^{\pi}_{\mathbf{k}\downarrow}$ by

$$A_{\mathbf{k}} = \frac{1}{L}\sum_{\mathbf{k}'} U^{S}_{\mathbf{k}\mathbf{k}'} \langle m_{\mathbf{k}'} \rangle \ , \tag{38}$$

where $U^{S}_{\mathbf{k}\mathbf{k}'} = \frac{1}{2}(U^{\sigma\sigma}_{\mathbf{k}\mathbf{k}'} - U^{\sigma,-\sigma}_{\mathbf{k}\mathbf{k}'})$. For a conventional commensurate antiferromagnet, $A_{\mathbf{k}}$ is real. The matrix $\mathcal{M}_{\mathbf{k}}$ then assumes the simpler structure

$$\mathcal{M}_{\mathbf{k}} = \begin{pmatrix} \xi_{\mathbf{k}} & \Delta_{\mathbf{k}} & A_{\mathbf{k}} & \Delta^{\pi}_{\mathbf{k}} \\ \Delta^{*}_{\mathbf{k}} & -\xi_{\mathbf{k}} & \Delta^{\pi *}_{\mathbf{k}+\mathbf{Q}} & A_{\mathbf{k}} \\ A_{\mathbf{k}} & \Delta^{\pi}_{\mathbf{k}+\mathbf{Q}} & \xi_{\mathbf{k}+\mathbf{Q}} & \Delta_{\mathbf{k}+\mathbf{Q}} \\ \Delta^{\pi *}_{\mathbf{k}} & A_{\mathbf{k}} & \Delta^{*}_{\mathbf{k}+\mathbf{Q}} & -\xi_{\mathbf{k}+\mathbf{Q}} \end{pmatrix} . \tag{39}$$

We have used reflection symmetry to replace $\xi_{-\mathbf{k}}$ by $\xi_{\mathbf{k}}$ etc.

In principle, the coexistence of antiferromagnetic order and superconductivity leads automatically to a finite $\pi$-pairing field.[23,24,34] To see this, consider the right hand side of the gap equation (35) for $\Delta^{\pi}_{\mathbf{k}}$. The relevant minor in the numerator can be written as

$$\det\big(M^{\lambda,41}_{\mathbf{k}}\big) = \Delta_{\mathbf{k}} A_{\mathbf{k}} (E^{\lambda}_{\mathbf{k}} - \xi_{\mathbf{k}+\mathbf{Q}}) + \Delta_{\mathbf{k}+\mathbf{Q}} A_{\mathbf{k}} (E^{\lambda}_{\mathbf{k}} + \xi_{\mathbf{k}}) \tag{40}$$

in the limit $\Delta^{\pi}_{\mathbf{k}} \to 0$. This is nonzero if both $A_{\mathbf{k}} \neq 0$ and $\Delta_{\mathbf{k}} \neq 0$. In other words, the coexistence of antiferromagnetic order and superconductivity generates a finite expectation value $\langle p^{\pi}_{\mathbf{k}} \rangle$. For a nonzero interaction in the $\pi$-pairing channel, $V^{\pi}_{\mathbf{k}\mathbf{k}'}$, this leads to a finite $\pi$-pairing field $\Delta^{\pi}_{\mathbf{k}}$. Since both $A_{\mathbf{k}}$ and $\Delta_{\mathbf{k}}$ are odd under spin flips, the spin flip symmetry of the expectation value $\langle p^{\pi}_{\mathbf{k}} \rangle$ generated by $A_{\mathbf{k}}$ and $\Delta^{\pi}_{\mathbf{k}}$ is even, corresponding to triplet pairing. This is why the interaction $V^{\pi}_{\mathbf{k}\mathbf{k}'}$ was extracted from the triplet component of the vertex in Eq. (15). In case of coexistence of superconductivity with a charge (instead of spin) density wave, the generated $\pi$-pairing would be odd under spin flips, and thus couples to the singlet vertex. Combined with the antisymmetry under particle exchange the spin flip symmetry of the $\pi$-pairing field yields the relation $\Delta^{\pi}_{\mathbf{k}} = -\Delta^{\pi}_{\mathbf{Q}-\mathbf{k}}$.

At and near half-filling, the dominant ordering tendencies of the two-dimensional Hubbard model are antiferromagnetism and singlet superconductivity. Under point group transformations the antiferromagnetic order parameter $A_{\mathbf{k}}$ has s-wave symmetry, while the superconducting gap $\Delta_{\mathbf{k}}$ has $\mathrm{d}_{x^2-y^2}$-symmetry. From Eq. (40) one can thus deduce that $\Delta^{\pi}_{\mathbf{k}}$ also has $\mathrm{d}_{x^2-y^2}$-symmetry. Note that the latter is not in conflict with the triplet spin symmetry of the $\pi$-pair, since the total momentum of the pair is $\mathbf{Q} = (\pi, \pi)$, not

zero. The effective interaction $\Gamma^{\Lambda}$ of the Hubbard model turns out to be very small in the triplet $\pi$-pairing channel, and its d-wave component is repulsive. Hence the $\pi$-pairing field $\Delta^{\pi}_{\mathbf{k}}$ is also very small compared to the other order parameters, such that its feedback into the gap equations for $A_{\mathbf{k}}$ and $\Delta_{\mathbf{k}}$ can be neglected.

## IV. RESULTS FOR THE TWO-DIMENSIONAL HUBBARD MODEL

In this section we present results obtained from the renormalized mean-field theory on antiferromagnetic order and superconductivity in the repulsive two-dimensional Hubbard model. We will first discuss antiferromagnetic states in the absence of superconductivity, then d-wave superconductivity in the absence of antiferromagnetic order, and finally the full theory allowing for coexistence. Superconductivity in the attractive Hubbard model is discussed briefly in Appendix B. All results will be presented for $t = 1$, that is, all quantities are given in units of $t$.

### A. Antiferromagnetism

In the absence of any other symmetry breaking, the gap equation for the antiferromagnetic order parameter $A_{\mathbf{k}}$ can be written as

$$A_{\mathbf{k}} = \frac{2}{L} \sum_{\mathbf{k}'} U^{S}_{\mathbf{k}\mathbf{k}'} \, \frac{A_{\mathbf{k}'}}{E^{+}_{\mathbf{k}'} - E^{-}_{\mathbf{k}'}} \, [f(E^{+}_{\mathbf{k}'} - f(E^{-}_{\mathbf{k}'})] \tag{41}$$

with the two quasi-particle energy branches

$$E^{\pm}_{\mathbf{k}} = \frac{\xi_{\mathbf{k}} + \xi_{\mathbf{k}+\mathbf{Q}}}{2} \pm \sqrt{\frac{1}{4}(\xi_{\mathbf{k}} - \xi_{\mathbf{k}+\mathbf{Q}})^2 + A^2_{\mathbf{k}}} \, . \tag{42}$$

For a dispersion relation due to nearest and next-to-nearest neighbor hopping one has

$$E^{\pm}_{\mathbf{k}} = \epsilon^{t'}_{\mathbf{k}} \pm \sqrt{(\epsilon^{t}_{\mathbf{k}})^2 + A^2_{\mathbf{k}}} - \mu \, , \tag{43}$$

where $\epsilon^{t}_{\mathbf{k}} = -2t(\cos k_x + \cos k_y)$ and $\epsilon^{t'}_{\mathbf{k}} = -4t' \cos k_x \cos k_y$ .

The antiferromagnetic order parameter affects the quasi-particle energies most strongly near the magnetic Brillouin zone boundary, since $\epsilon^{t}_{\mathbf{k}}$ vanishes there. The dispersion of the two branches $E^{\pm}_{\mathbf{k}}$ along this line is shown in Fig. 4 for a constant (momentum independent) $A_{\mathbf{k}}$ and $t' < 0$. Note that the momentum dependence of $A_{\mathbf{k}}$ is indeed rather weak in our RG+MF calculations. Within plain mean-field theory applied to the Hubbard model one has $U^{S}_{\mathbf{k}\mathbf{k}'} = -U/2$ so that $A_{\mathbf{k}}$ is completely momentum independent. The antiferromagnetic mean-field theory has been applied to the two-dimensional Hubbard model in several earlier works.[37,38,39,40]

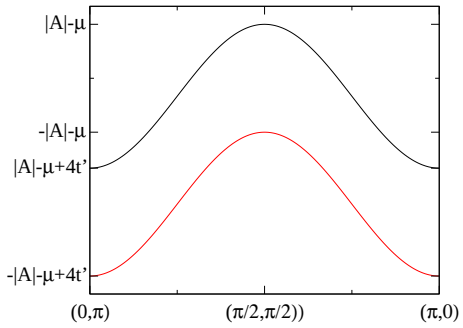


FIG. 4: (Color online) Dispersion of quasi-particle energies $E^{\pm}_{\mathbf{k}}$ on the magnetic Brillouin zone boundary ("umklapp surface") in the antiferromagnetic state for a momentum independent $A_{\mathbf{k}}$ and $t' < 0$.

The two branches $E^{+}_{\mathbf{k}}$ and $E^{-}_{\mathbf{k}}$ are separated by a global energy gap if $|A_{\mathbf{k}}| > 2|t'|$. If the chemical potential lies in that gap, such that $E^{+}_{\mathbf{k}} > 0$ and $E^{-}_{\mathbf{k}} < 0$ for all $\mathbf{k}$, the electron density is at half-filling and the system does not exhibit any gapless excitations. Gapless excitations do exist if $E^{+}_{\mathbf{k}}$ or $E^{-}_{\mathbf{k}}$ has zeros. The equations $E^{\pm}_{\mathbf{k}} = 0$ define effective Fermi surfaces of the antiferromagnetic state. From Figs. 4 and 5 one can see that for $t' < 0$ and close to half-filling the effective Fermi surfaces enclose hole pockets in the branch $E^{-}_{\mathbf{k}}$ around $(\pi/2, \pi/2)$ and electron pockets in $E^{+}_{\mathbf{k}}$ around $(\pi, 0)$ and $(0, \pi)$. Similar effective

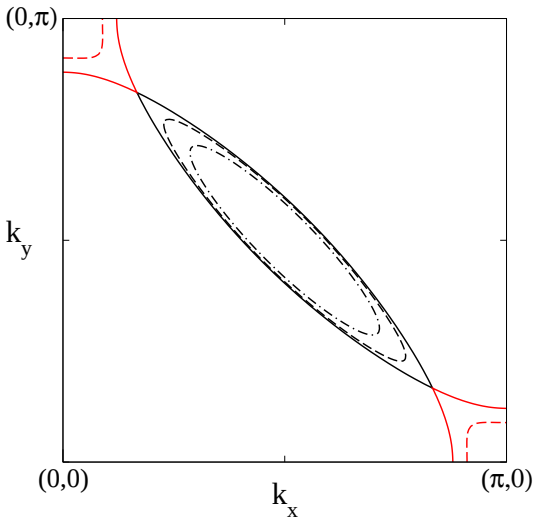


FIG. 5: (Color online) Effective Fermi surfaces in the antiferromagnetic state for $t' = -0.2$, $\mu = -0.6$, and various momentum independent choices of the antiferromagnetic gap function $A_{\mathbf{k}}$: 0 (solid line), 0.15 (dashed line), 0.3 (dashed-dotted line).

Fermi surfaces are obtained in a d-density wave state.[41] For a momentum independent antiferromagnetic gap function $A_{\mathbf{k}}$ the separatrices between states with hole pockets, electron pockets and fully gapped states are given by simple linear combinations of the

parameters $t'$, $\mu$ and $A$. For a fixed $t' < 0$ the various regimes in the plane spanned by $\mu$ and $A$ are shown in Fig. 6. Note the special point given by $\mu_{1/2} = A = 2t'$ at which the

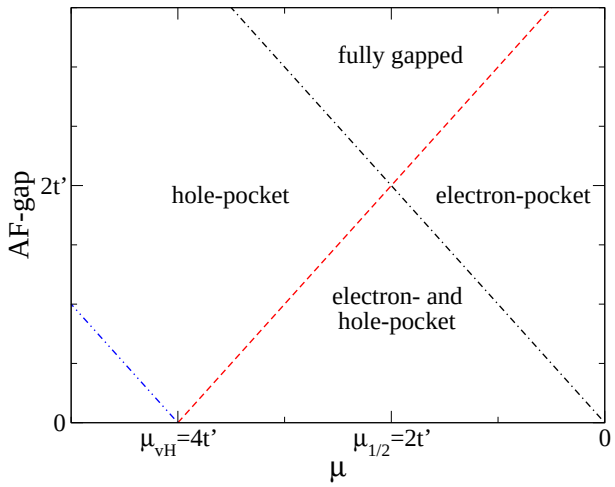


FIG. 6: (Color online) Topology of the effective Fermi surfaces in the plane spanned by the chemical potential $\mu$ and the antiferromagnetic gap $A$. No Fermi surface exists in the fully gapped regime.

separatrices for electron and hole pockets cross each other. For $\mu < \mu_{\rm vH}$ and a small $A_{\mathbf{k}}$ the effective Fermi surface is closed around $(0, 0)$ and does not intersect with the magnetic Brillouin zone boundary.

A typical mean-field result for the $\mu$-dependence of the antiferromagnetic gap in the Hubbard model is shown in Fig. 7. The coupling strength $U$ has been chosen sufficiently

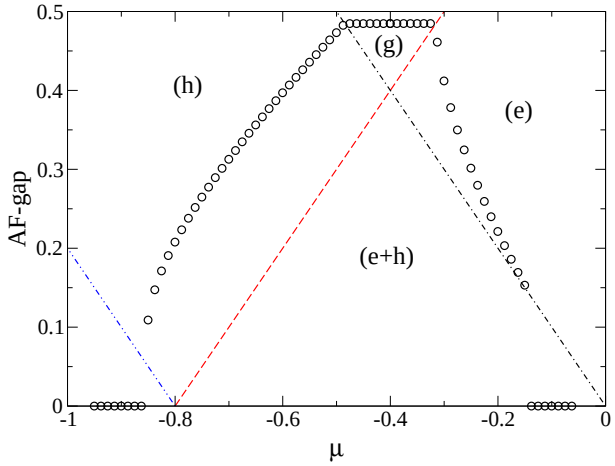


FIG. 7: (Color online) Mean-field solution for the antiferromagnetic gap as a function of $\mu$ for the Hubbard model with $t' = -0.2$ and $U = 2.25$. Regions with different Fermi surface topology are indicated as in Fig. 6.

large to stabilize fully gapped half-filled solutions for $\mu$ near $\mu_{1/2}$. The antiferromagnetic

order parameter vanishes discontinuously at the edges of the antiferromagnetic region. The effective Fermi surface of the antiferromagnetic states consists (exclusively) of hole pockets for hole doping and of electron pockets for electron doping. For other finite values of $t'$ the $\mu$-dependence of $A_{\mathbf{k}}$ is qualitatively the same for sufficiently large $U$.

For $t' = 0$ half-filled fully gapped antiferromagnetic solutions are stabilized for any (arbitrarily small) $U$, but no stable antiferromagnetic solutions away from half-filling exist. Solutions of the self-consistency equations leading to densities away from half-filling correspond to maxima (instead of minima) in the free energy and are therefore physically irrelevant.[36,42] If a certain density near half-filling is enforced, the system will thus phase separate in a half-filled antiferromagnetic and a non-half-filled paramagnetic region.

We now turn to results obtained from the combined RG+MF theory described in the preceeding sections. The effective interaction $U^S_{\mathbf{k}\mathbf{k}'}$ driving the antiferromagnetic order is computed from the RG flow integrated down to a cutoff scale $\Lambda_{\rm MF}$, and the momentum space entering the mean-field equations is correspondingly restricted by this cutoff. Since the mode elimation is done only approximately both above and below $\Lambda_{\rm MF}$, the choice of $\Lambda_{\rm MF}$ will affect the accuracy of the final results. In Fig. 8 we show the dependence of the antiferromagnetic gap function $A_{\mathbf{k}}$ on $\Lambda_{\rm MF}$ for the perfect nesting case ($t' = 0$ at half-filling) with a relatively weak bare coupling strength $U = 2$. The different curves correspond to momenta $\mathbf{k}$ in six different patches interpolating between the $k_x$ or $k_y$ axis (patch 1) and the Brillouin zone diagonal (patch 6), see also Fig. 2. The patch-dependence is relatively weak, reflecting the weak momentum dependence of $A_{\mathbf{k}}$. Fluctuations cap-

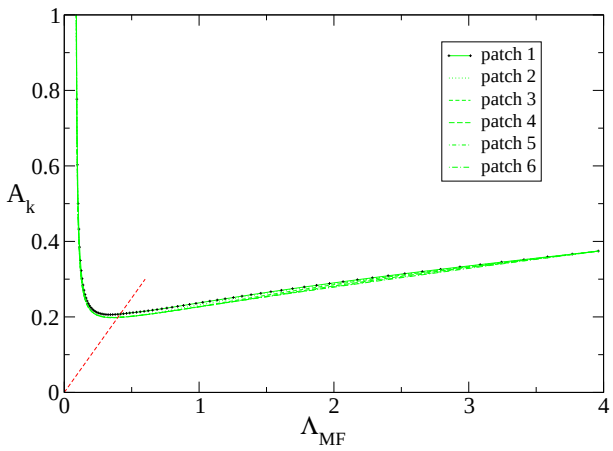


FIG. 8: (Color online) Antiferromagnetic gap as a function of the cutoff $\Lambda_{\rm MF}$ for the Hubbard model with pure nearest neighbor hopping ($t' = 0$) and $U = 2$ at half-filling. Due to the weak momentum dependence of $A_{\mathbf{k}}$ the curves corresponding to different patches are very close to each other. The intersection of the largest $A_{\mathbf{k}}$ (patch 1) with the straight line given by $\Lambda_{\rm MF} = 2A_{\mathbf{k}}$ yields at suitable choice of $\Lambda_{\rm MF}$ leading to a reasonable estimate of the true gap size.

tured by the one-loop RG flow reduce the size of $A_{\mathbf{k}}$ compared to the plain mean-field result (corresponding to $\Lambda_{\rm MF} = \Lambda_0 = 4$). This reduction is expected and can also be obtained by a suitable perturbation theory for the symmetry-broken state.[43,44] Within mean-field theory, the effective interaction is driven exclusively by one-loop diagrams in the antiferromagnetic particle-hole channel, leading to an enhancement compared to the bare interaction. In the full one-loop flow other contributions, especially from the particle-particle channel, reduce this enhancement, leading to a smaller $A_{\mathbf{k}}$.

The size of $A_{\mathbf{k}}$ saturates at low $\Lambda_{\rm MF}$ until it is pushed upwards by a strong divergence at a cutoff scale of the order of the gap size just before the upturn. This divergence reflects the breakdown of the one-loop approximation at the energy scale of symmetry breaking. The renormalized interaction becomes strong at that scale and the influence of the antiferromagnetic order parameter on the flow becomes crucial. The latter is captured by the mean-field theory, which is definitely a better approximation at scales of the order of the final gap. The one-loop flow without order parameter feedback fails even in pure mean-field models at the scale where symmetry breaking sets in. Hence we have to stop the one-loop flow at a scale safely above the scale of symmetry breaking. On the other hand one would like to capture the one-loop fluctuations not treated in mean-field theory down to the lowest possible scales. Unfortunately there is no unique choice of an "optimal" $\Lambda_{\rm MF}$. In the following we will stop the one-loop flow at a scale $\Lambda_{\rm MF}$ which is twice as big as the largest (as a function of $\mathbf{k}$) gap value in the symmetry-broken state obtained from the mean-field theory for the states below $\Lambda_{\rm MF}$. The relation $\Lambda_{\rm MF} = 2A_{\mathbf{k}}$ corresponds to the straight line in Fig. 8. The estimate for $A_{\mathbf{k}}$ is obtained from the intersection of that line with the largest $A_{\mathbf{k}}$, that is, the ones with $\mathbf{k}$ on patch 1. In the present case this estimate is rather robust with respect to slight shifts of $\Lambda_{\rm MF}$.

### B. d-wave superconductivity

It is well known that the one-loop RG flow generates an attractive interaction in the d-wave Cooper channel.[12,13,14,15] Although antiferromagnetic fluctuations contribute significantly to this attraction, the Cooper instability ultimately competes with antiferromagnetism. In Fig. 9 we show results for the superconducting gap function $\Delta_{\mathbf{k}}$ as a function of the cutoff $\Lambda_{\rm MF}$ in the RG+MF scheme. Different curves correspond to different patches, as in Fig. 8. The parameters have been chosen such that the antiferromagnetic interaction is too weak to drive antiferromagnetic order. Within plain mean-field theory no superconductivity is obtained since the bare (repulsive) Hubbard interaction is repulsive in the s-wave Cooper channel and vanishes for any other symmetry. Hence $\Delta_{\mathbf{k}}$ vanishes for $\Lambda_{\rm MF}$ at the band edge and increases monotonically upon lowering $\Lambda_{\rm MF}$. The pronounced momentum dependence of $\Delta_{\mathbf{k}}$ reflects the $d_{x^2-y^2}$ symmetry. As in the case of antiferromagnetism, $\Delta_{\mathbf{k}}$ diverges if the one-loop flow is continued below scales of the

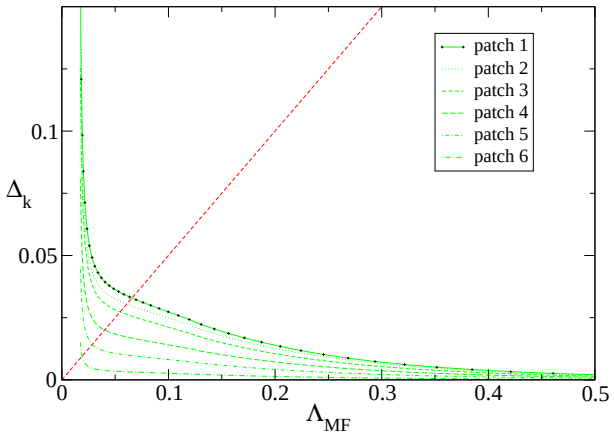


FIG. 9: (Color online) Superconducting gap as a function of the cutoff $\Lambda_{\rm MF}$ for the Hubbard model in a regime where superconductivity is the only instability. Parameters: $U = 2.5$, $t' = -0.2$, $\mu = -0.9265$.

order of the gap amplitude. A reasonable choice of $\Lambda_{\rm MF}$ is obtained from the condition $\Lambda_{\rm MF} = 2\Delta_{\mathbf{k}}$ (straight line in Fig. 9) applied to the largest $\Delta_{\mathbf{k}}$ (patch 1). As long as one does not approach the divergence, the result for $\Delta_{\mathbf{k}}$ does not depend too much on the precise choice of $\Lambda_{\rm MF}$.

### C. Antiferromagnetism and superconductivity

We now analyze the competition between antiferromagnetism and superconductivity within the full RG+MF theory, where both types of order and also the possibility of their coexistence are allowed. We focus on the case $t' < 0$, which is realized in particular in the cuprate superconductors. We restrict ourselves to densities at and below half-filling.

In Fig. 10 we show results from the RG+MF calculation for the amplitudes of the d-wave superconducting gap $\Delta_{\mathbf{k}}$ and the antiferromagnetic gap $A_{\mathbf{k}}$ as a function of the chemical potential $\mu$, and in Fig. 11 as a function of the electron density. The latter is computed simultaneously with the order parameters and differs from the bare density corresponding to $\mu$. The interaction $U = 2.5$ is strong enough to stabilize an antiferromagnetic insulator at half-filling, in spite of the magnetic frustration induced by the next-to-nearest neighbor hopping $t' = -0.15$. The system is fully gapped at half-filling and the superconducting order parameter is strictly zero there. With decreasing filling the antiferromagnetic gap decreases monotonically, while $\Delta_{\mathbf{k}}$ remains numerically zero. For electron densities below one, holes appear first in pockets around $(\pi/2, \pi/2)$, which define a surface of low-energy excitations of the non-half filled system. In principle, this residual Fermi surface is always unstable against superconductivity, due to the attractive interaction in the d-wave Cooper channel. However, very close to half-filling, where

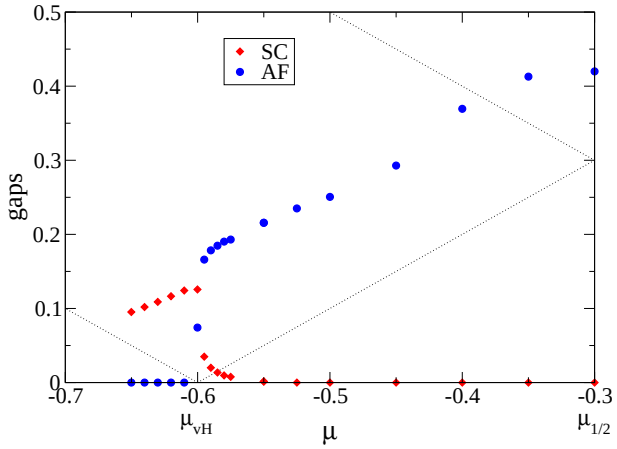


FIG. 10: (Color online) Amplitudes of the superconducting gap $\Delta_{\mathbf{k}}$ and the antiferromagnetic gap $A_{\mathbf{k}}$ as a function of $\mu$ for $U = 2.5$ and $t' = -0.15$. The dotted lines are the separatrices between different Fermi surface topologies as specified in Fig. 6.

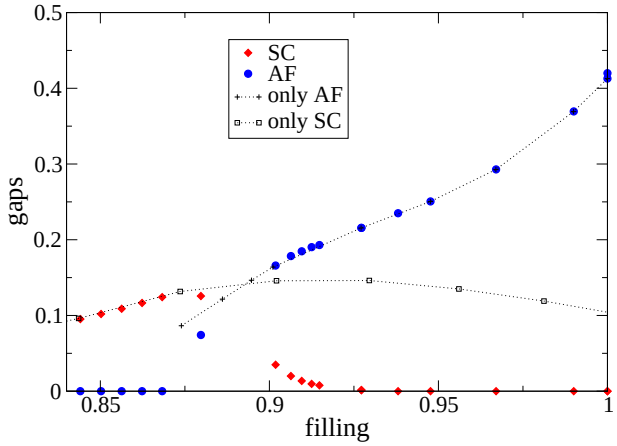


FIG. 11: (Color online) Amplitudes of $\Delta_{\mathbf{k}}$ and $A_{\mathbf{k}}$ as a function of density for $U = 2.5$ and $t' = -0.15$. Filled colored symbols represent the results obtained for the combined theory with two order parameters, while in the results represented by open symbols only one order parameter, either antiferromagnetic or superconducting, was allowed in the mean-field calculation. The two slightly different results for the antiferromagnetic gap at half-filling correspond to two different choices of $\mu$ within the gap; this $\mu$-dependence is an artefact of the approximations.

the pockets are small, the superconducting gap is tiny, since the d-wave attraction is very small near the Brillouin zone diagonal. When the hole pockets are large enough, roughly for $n < 0.92$, a sizeable superconducting gap develops, coexisting with a finite antiferromagnetic order parameter. When $\mu$ approaches $\mu_{\rm vH}$, the antiferromagnetic gap decreases rapidly. This leads also to a very fast decrease of the electron density (see Fig. 11) as a function of decreasing $\mu$. The antiferromagnetic gap vanishes for $\mu < \mu_{\rm vH}$,

while $\Delta_{\mathbf{k}}$ remains finite and decreases monotonically with decreasing filling. Note that the antiferromagnetic transition is not generically situated as close to $\mu_{\rm vH}$ as in Fig. 10.

The numerical analysis is rather involved in the coexistence region and we have not clarified the nature of the magnetic transition (first or steep second order). The presence of the superconducting gap makes the magnetic transition smoother, but whether this effect is big enough to yield a continuous transition is not clear from the numerical data. In any case, fluctuations which have been neglected in the mean-field approximation are expected to play an important role in the transition region and may even affect the order of the transition.

The respective results for each order parameter when the other one is set to zero are also shown in Fig. 11. When $A_{\mathbf{k}}$ is set to zero, the superconducting gap $\Delta_{\mathbf{k}}$ persists even at half filling. When $\Delta_{\mathbf{k}}$ is set to zero, the antiferromagnetic order parameter is enhanced in the coexistence region. In both cases a finite value for one order parameter leads to a suppression of the other. While these results have been obtained for a weak on-site repulsion, they are in line with the behavior at stronger coupling as obtained by the variational Monte Carlo technique,[45] by cluster and cellular dynamical mean-field theory,[46,47] and by variational cluster approximations[48,49] for the two-dimensional Hubbard model. The regime of substantial coexistence of antiferromagnetic order and superconductivity obtained in those calculations is typically larger than in our results. However, in the cluster calculations the amount of coexistence seems to depend sensitively on the cluster size.[48] In a recent cellular dynamical mean-field calculation with a 2x2 cluster it was found that coexistence is not possible if $U$ exceeds the band width.[47]

In Fig. 12 we show the angular dependence of $\Delta_{\mathbf{k}}$ and $A_{\mathbf{k}}$ for three selected densities, along with the corresponding effective Fermi surfaces. The angle $\phi$ is defined with respect to the $k_x$ axis. For $n = 0.99$ we obtain a sizable antiferromagnetic gap which has s-wave symmetry and is slightly anisotropic. The superconducting gap is practically zero. The hole pocket enclosed by the effective Fermi surface is rather small and does not support a sizable superconducting gap. For $n = 0.906$ we observe a coexistence of both order parameters. While $A_{\mathbf{k}}$ is reduced in size compared to the case $n = 0.99$, its shape remains essentially the same. The hole pocket extends further away from the Brillouin zone diagonal and allows for a substantial superconducting gap with d-wave symmetry. In this situation the low-energy excitations are gapped due to $A_{\mathbf{k}}$ near the points $(\pi, 0)$ and $(0, \pi)$, and due to $\Delta_{\mathbf{k}}$ along the hole pocket, with nodes along the Brillouin zone diagonal. For the even smaller density $n = 0.862$ the antiferromagnetic order parameter vanishes and only a d-wave superconducting gap remains, which extends over the whole Fermi surface except at the nodal points. Note that the momentum dependence of the gap function has peaks near the van Hove points and is relatively flat near the Brillouin zone diagonal, implying that terms beyond the lowest d-wave harmonic $\cos k_x - \cos k_y$ contribute significantly to $\Delta_{\mathbf{k}}$.

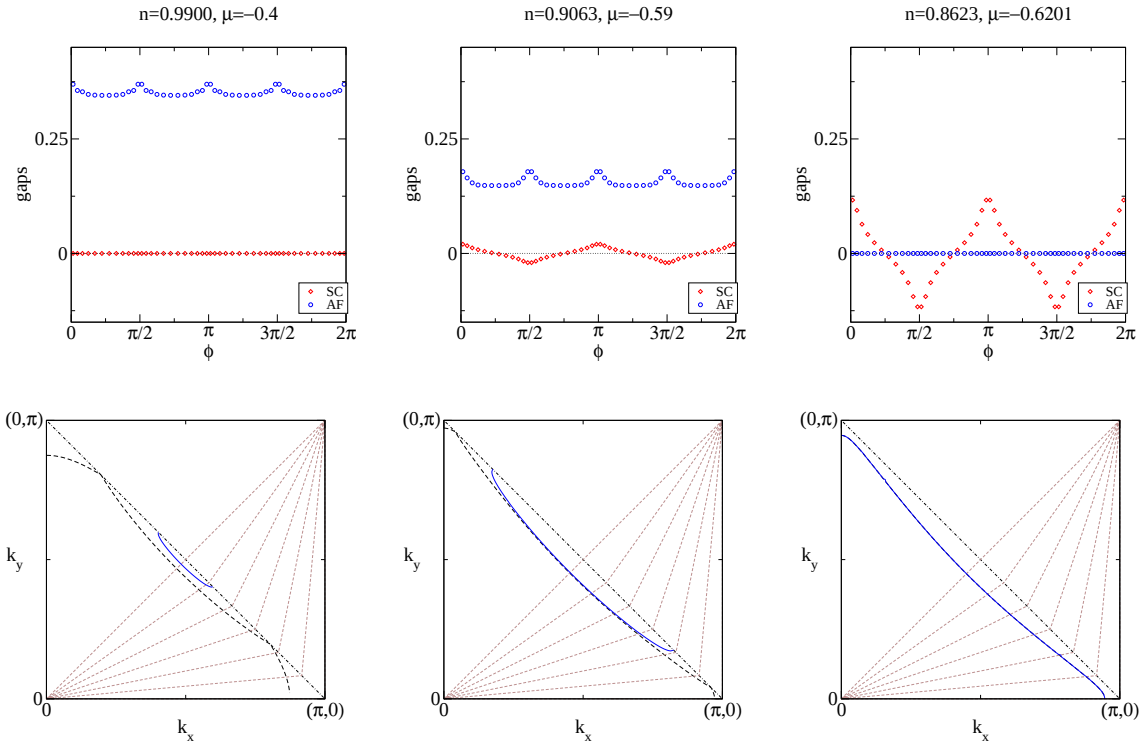


FIG. 12: (Color online) *Top*: Angular dependence of the d-wave superconducting and antiferromagnetic order parameters at three different values of the chemical potential. *Bottom*: Fermi surfaces in the magnetic Brillouin zone (solid blue lines); in the antiferromagnetic state close to half-filling the Fermi surface forms a hole pocket around $(\pi/2, \pi/2)$. The corresponding bare Fermi surfaces, backfolded with respect to Umklapp surface, are shown as broken lines. The straight lines indicate the patching scheme. The parameters $U = 2.5$ and $t' = -0.15$ are the same as in Figs. 10 and 11.

In Figs. 10-12 the coupling strength $U$ has been chosen such that three different states, that is, antiferromagnetic insulator, doped antiferromagnet coexisting with superconductivity, and a pure d-wave superconductor could be obtained for different choices of $\mu$. By contrast, for a sufficiently small $U$ (at finite $t'$) the system is a d-wave superconductor for any $\mu$. On the other hand, for large $U$ the system is an antiferromagnet near half-filling and switches to a purely superconducting state if the chemical potential descends below a certain critical value. The superconducting gap in the doped antiferromagnet remains tiny for large $U$. A global view of the $U$ and $\mu$-dependences is presented in Fig. 13, where we show the ground state phase diagram of the two-dimensional Hubbard model in the $\mu$-$U$ plane for a fixed $t' = -0.1$. Note that the parameter region supporting substantial coexistence of antiferromagnetism and superconductivity is rather narrow. For $U = 1.75$ and $U = 2$, antiferromagnetic order is stabilized only *below* half-filling.

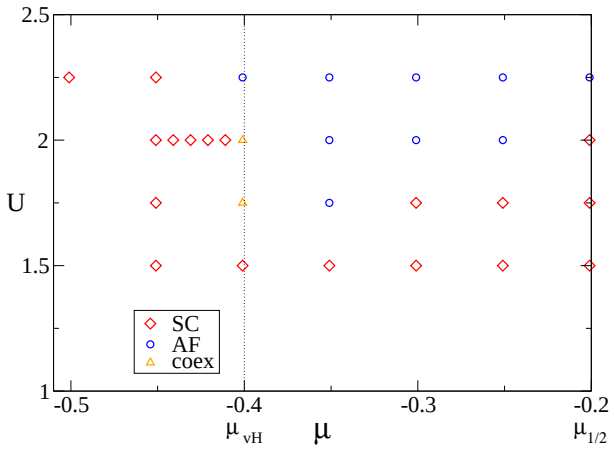


FIG. 13: (Color online) Points with antiferromagnetism, superconductivity and coexistence of both in the $\mu$-$U$ plane for a fixed $t' = -0.1$; "coexistence" means that the amplitude of $\Delta_{\mathbf{k}}/A_{\mathbf{k}}$ is at least $10^{-3}$.

## V. CONCLUSION

We have analyzed the competition between antiferromagnetism and superconductivity in the two-dimensional Hubbard model by combining a functional RG flow with a mean-field theory for symmetry-breaking. Effective interactions were computed by integrating out states with an energy above a scale $\Lambda_{\rm MF}$ via a one-loop RG flow, which captures in particular the generation of an attractive interaction in the d-wave Cooper channel from fluctuations in the particle-hole channel.[12,13,14] These effective interactions were then used as an input for a mean-field treatment of the remaining states, below the scale $\Lambda_{\rm MF}$, with commensurate antiferromagnetism, singlet superconductivity, and triplet $\pi$-pairing as the possible order parameters. Triplet $\pi$-pairing appears generically when antiferromagnetism and singlet superconductivity coexist.[34] Our theory extends previous mean-field treatments of antiferromagnetism and d-wave superconductivity, where the effective interactions were specified by a relatively simple ansatz with a few input parameters, or they were identified with bare interactions of a microscopic model.[22,23,24,25] In the present work the size and shape (momentum dependence) of the effective interactions were actually *computed*, within an approximation that captures fluctuations and is controlled at weak coupling.

It turned out that the feedback of $\pi$-pairing on the other order parameters is negligble for the two-dimensional Hubbard model. The key players, antiferromagnetism and d-wave superconductivity, strongly compete. For a sufficiently large $U$ (depending on the size of $t'$) an antiferromagnetic insulator is stabilized at half-filling, as expected. Doping the antiferromagnet with holes (for $t' < 0$) leads to an effective Fermi surface with hole pockets around $(\pi/2, \pi/2)$. In principle, these give rise to a superconducting instability,

but the corresponding gap is usually tiny. At larger doping the antiferromagnetism breaks down and d-wave superconductivity prevails. There is a small range of densities where both orders can coexist with a sizable order parameter for each.

Coexistence of antiferromagnetism and superconductivity in the two-dimensional Hubbard model has also been obtained by the variational Monte Carlo technique,[45] by cluster and cellular dynamical mean-field theory,[46,47] and by variational cluster approximations.[48,49] Coexistence has also been observed in some cuprate high-temperature superconductors in the underdoped regime.[50,51]

We have restricted our analysis of symmetry breaking to superconductivity and commensurate antiferromagnetism, while in principle also other instabilities may arise. The most serious candidates (and difficult to treat) are probably the various possibilities of incommensurate magnetic order in the low doping regime.[38,39] For the two-dimensional t-J model with a finite $t'$ it was shown that for very low doping a spiral phase is stabilized and that superconductivity develops in the spiral state.[52] Another possibility is the formation of a d-density wave, that is, a charge density wave with a wave vector near $(\pi, \pi)$ and a form factor with d-wave symmetry.[53,54] This ordered phase is known to occur in a suitable large $N$ extension of the t-J model, where it competes and partially coexists with d-wave superconductivity.[53] Renormalization group calculations for the two-dimensional Hubbard model yield enhanced d-density wave correlations, but the antiferromagnetic and superconducting instabilities are stronger.[55]

A more complete analysis of the two-dimensional Hubbard model by renormalization group methods, including also order parameter fluctuations at low energy scales, can be expected to yield further important clues for a better understanding of the interplay of magnetism and superconductivity.

**Acknowledgments**

We thank R. Gersch, C. Honerkamp, A. Katanin, M. Salmhofer, P. Strack, O. Sushkov, and R. Zeyher for valuable discussions.

## APPENDIX A: DERIVATION OF GAP EQUATIONS

Let $\phi_{\mathbf{k}}$ be any of the expectation values $\langle n_{\mathbf{k}\sigma}\rangle$, $\langle n^{\pi}_{\mathbf{k}\sigma}\rangle$, $\langle p_{\mathbf{k}}\rangle$, $\langle p^{\pi}_{\mathbf{k}}\rangle$, or their complex conjugates. Applying the necessary condition for a minimum, $\partial\Omega/\partial\phi_{\mathbf{k}} = 0$, to $\Omega$ in Eq. (30) yields

$$\frac{\partial K^c}{\partial \phi_{\mathbf{k}}} + \sum_{\mathbf{k}'} \sum_{\lambda} \frac{\partial E^{\lambda}_{\mathbf{k}'}}{\partial \phi_{\mathbf{k}}} f(E^{\lambda}_{\mathbf{k}'}) = 0 \tag{A1}$$

The derivatives of the energy eigenvalues $E^{\lambda}_{\mathbf{k}'}$ can be expressed in terms of minors $\det(M^{\lambda,jj'}_{\mathbf{k}'})$ of $\mathcal{M}^{\lambda}_{\mathbf{k}'}$ and matrix elements $(\mathcal{M}_{\mathbf{k}'})_{jj'}$ of $\mathcal{M}_{\mathbf{k}'}$ as

$$\frac{\partial E^{\lambda}_{\mathbf{k}'}}{\partial \phi_{\mathbf{k}}} = \frac{1}{\sum_l \det\big(M^{\lambda,ll}_{\mathbf{k}'}\big)} \sum_{j,j'} \frac{\partial (\mathcal{M}_{\mathbf{k}'})_{jj'}}{\partial \phi_{\mathbf{k}}} \, (-1)^{j-j'} \det\big(M^{\lambda,jj'}_{\mathbf{k}'}\big) \; . \tag{A2}$$

This follows from acting with $\partial/\partial\phi_{\mathbf{k}}$ on the equation for the eigenvalues $\det\big(\mathcal{M}_{\mathbf{k}'} - E^{\lambda}_{\mathbf{k}'}\mathbf{1}\big) = 0$ and the rule for derivatives of determinants

$$\frac{\partial}{\partial \phi} \det(M) = \sum_{j,j'} \frac{\partial (M)_{jj'}}{\partial \phi} \, (-1)^{j-j'} \det(M^{jj'}) \; . \tag{A3}$$

The gap equations are now obtained by taking the specific derivatives for each case. Terms differing only by a momentum shift $\mathbf{Q}$ can be summed up by using the identities $E^{\lambda}_{\mathbf{k}+\mathbf{Q}} = E^{\lambda}_{\mathbf{k}}$ and $\det\big(M^{\lambda,jj'}_{\mathbf{k}+\mathbf{Q}}\big) = \det\big(M^{\lambda,j+2,j'+2}_{\mathbf{k}}\big)$, with $j+2$ and $j'+2$ modulo 4, which follow from the block structure (27) of $\mathcal{M}_{\mathbf{k}}$.

To derive Eq. (36) we start from Kramer's rule for matrix inversion in terms of minors, $\det(M)\,(M^{-1})_{ll'} = (-1)^{l-l'}\det(M^{l'l})$. Summing the diagonal elements yields $\sum_l \det(M^{ll}) = \det(M)\,\mathrm{tr}(M^{-1})$. Expressing the trace and the determinant by the eigenvalues $m_\alpha$ of $M$ yields $\sum_l \det(M^{ll}) = \sum_\alpha \prod_{\alpha' \neq \alpha} m_{\alpha'}$. If one of the eigenvalues, say $m_\lambda$, vanishes, only the term $\alpha = \lambda$ contributes, yielding $\sum_l \det(M^{ll}) = \prod_{\lambda' \neq \lambda} m_{\lambda'}$. Applying this identity to the matrix $\mathcal{M}^{\lambda}_{\mathbf{k}}$ one obtains directly Eq. (36).

## APPENDIX B: ATTRACTIVE HUBBARD MODEL

In the attractive Hubbard model away from half-filling only the Cooper channel leads to an instability, namely s-wave superconductivity.[56] All other channels yield just finite renormalizations. In Fig. 14 we show the dependence of the superconducting gap on $\Lambda_{\mathrm{MF}}$ as obtained from the RG+MF theory for the attractive Hubbard model with $U = -1.5$ and $t' = -0.1$ at quarter-filling. As in the case of antiferromagnetism in the repulsive model, the gap size is reduced by fluctuations compared to the mean-field result. For $\Lambda$ between $4-\mu \approx 6$ and $4+\mu \approx 2$ only states above the Fermi level are integrated out, while states below the Fermi level are captured only for smaller $\Lambda$. This is the reason for the kink in $\Delta_{\mathbf{k}}$ at $\Lambda_{\mathrm{MF}} = 4+\mu$. The gap diverges at a critical scale $\Lambda_c$ due to the breakdown of the one-loop approximation discussed already in Sec. IV A. For $\Lambda_c \ll \Lambda_{\mathrm{MF}} \ll 1$ the dependence of $\Delta_{\mathbf{k}}$ on $\Lambda_{\mathrm{MF}}$ is relatively weak. This is the regime where the cutoff is still high enough so that the one-loop approximation is still accurate, but on the other hand already sufficiently low so that the flow of the effective interaction $V_{\mathbf{k}\mathbf{k}'}$ is dominated by the particle-particle channel, such that interactions beyond the reduced (mean-field) model

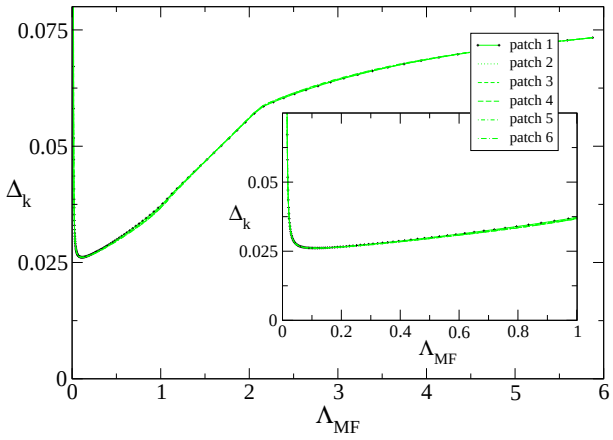


FIG. 14: (Color online) Superconducting gap $\Delta_{\mathbf{k}}$ as a function of the cutoff $\Lambda_{\mathrm{MF}}$ for the attractive Hubbard model ($U = -1.5$, $t' = -0.1$) at quarter-filling. Due to the weak momentum dependence of $\Delta_{\mathbf{k}}$ curves corresponding to different patches lie almost on top of each other. The inset shows $\Delta_{\mathbf{k}}$ for $\Lambda_{\mathrm{MF}} \leq 1$ with a higher resolution.

are irrelevant.

---


[1] P. W. Anderson, Science **235**, 1196 (1987).

[2] See, for example, D. J. Scalapino, Phys. Rep. **250**, 329 (1995).

[3] K. Miyake, S. Schmitt-Rink, and C. M. Varma, Phys. Rev. B **34**, 6554 (1986).

[4] D. J. Scalapino, E. Loh, and J. E. Hirsch, Phys. Rev. B **34**, 8190 (1986).

[5] N. E. Bickers, D. J. Scalapino, and R. T. Scalettar, Int. J. Mod. Phys. B **1**, 687 (1987).

[6] N. E. Bickers, D. J. Scalapino, and S. R. White, Phys. Rev. Lett. **62**, 961 (1989).

[7] For reviews of numerical work, see E. Dagotto, Rev. Mod. Phys. **66**, 763 (1994); N. Bulut, Adv. Phys. **51**, 1587 (2002).

[8] H. J. Schulz, Europhys. Lett. **4**, 609 (1987).

[9] I. Dzyaloshinskii, Sov. Phys. JETP **66**, 848 (1987).

[10] P. Lederer, G. Montambaux, and D. Poilblanc, J. Phys. (Paris) **48**, 1613 (1987).

[11] For a short review of functional RG techniques for interacting Fermi systems and applications, see W. Metzner, Prog. Theor. Phys. Suppl. **160**, 58 (2005).

[12] D. Zanchi and H. J. Schulz, Z. Phys. B **103**, 339 (1997); Europhys. Lett. **44**, 235 (1998); Phys. Rev. B **61**, 13609 (2000).

[13] C. J. Halboth and W. Metzner, Phys. Rev. B **61**, 7364 (2000).

[14] C. Honerkamp, M. Salmhofer, N. Furukawa, and T.M. Rice, Phys. Rev. B **63**, 035109 (2001).

[15] A.P. Kampf and A.A. Katanin, Phys. Rev. B **67**, 125104 (2003).

[16] J. Feldman, J. Magnen, V. Rivasseau, and E. Trubowitz, *Europhys. Lett.* **24**, 437 (1993).

[17] C. J. Halboth and W. Metzner, Phys. Rev. Lett. **85**, 5162 (2000).

[18] M. Salmhofer, C. Honerkamp, W. Metzner, and O. Lauscher, Prog. Theor. Phys. **112**, 943 (2004).

[19] R. Gersch, C. Honerkamp, D. Rohe, and W. Metzner, Eur. Phys. J. B **48**, 349 (2005).

[20] T. Baier, E. Bick, and C. Wetterich, Phys. Rev. B **70**, 125111 (2004).

[21] W. Metzner, J. Reiss, and D. Rohe, Phys. stat. sol. **243**, 46 (2006).

[22] M. Inui, S. Doniach, P.J. Hirschfeld, and A.E. Ruckenstein, Phys. Rev. B **37**, 2320 (1988).

[23] M. Murakami and H. Fukuyama, J. Phys. Soc. Jpn. **67**, 2784 (1998).

[24] B. Kyung, Phys. Rev. B **62**, 9083 (2000).

[25] H. Yamase and H. Kohno, Phys. Rev. B **69**, 104526 (2004).

[26] K.G. Wilson and J. Kogut, Phys. Rep. C **12**, 75 (1974).

[27] For a pedagogical introduction, see R. Shankar, Rev. Mod. Phys. **66**, 129 (1994).

[28] M. Salmhofer, *Renormalization: An Introduction* (Springer, Heidelberg, 1999).

[29] M. Salmhofer and C. Honerkamp, Prog. Theor. Phys. **105**, 1 (2001).

[30] C. Honerkamp, D. Rohe, S. Andergassen, and T. Enss, Phys. Rev. B **70**, 235115 (2004).

[31] J. Polchinski, Nucl. Phys. B **231**, 269 (1984).

[32] Spontaneous symmetry breaking is not always signalled by divergent interactions; in case of first order transitions they usually remain finite.

[33] H. Yamase and H. Kohno, J. Phys. Soc. Jpn. **69**, 332 (2000); **69**, 2151 (2000).

[34] G.C. Psaltakis and E.W. Fenton, J. Phys. C **16**, 3913 (1983).

[35] For the reduced BCS model, for example, it was shown already long ago that mean-field theory becomes exact in the thermodynamic limit, see B. Mühlschlegel, J. Math. Phys. **3**, 522 (1962).

[36] J. Reiss, Ph.D. thesis, Universität Stuttgart (2006).

[37] H.Q. Lin and J.E. Hirsch, Phys. Rev. B **35**, 3359 (1987).

[38] H. J. Schulz, Phys. Rev. Lett. **64**, 1445 (1990).

[39] A.V. Chubukov and D.M. Frenkel, Phys. Rev. B **46**, 11884 (1992).

[40] W. Hofstetter and D. Vollhardt, Ann. Physik **7**, 48 (1998).

[41] A. Greco and R. Zeyher, Phys. Rev. B **70**, 024518 (2004).

[42] The absence of stable solutions with broken symmetry away from half-filling is also found in a mean-field model for commensurate charge density waves, see R. Gersch, J. Reiss, and C. Honerkamp, cond-mat/0609520.

[43] A. Georges and J.S. Yedidia, Phys. Rev. B **43**, 3475 (1991).

[44] P.G.J. van Dongen, Phys. Rev. Lett. **67**, 757 (1991).

[45] T. Giamarchi and C. Lhuillier, Phys. Rev. B **43**, 12943 (1991).

[46] A.I. Lichtenstein and M.I. Katsnelson, Phys. Rev. B **62**, 9283 (2000).

[47] M. Capone and G. Kotliar, Phys. Rev. B **74**, 054513 (2006).

[48] D. Sénéchal, P.-L. Lavertu, M.-A. Marois, and A.-M.S. Tremblay, Phys. Rev. Lett. **94**, 156404

(2005).

[49] M. Aichhorn, E. Arrigoni, M. Potthoff, and W. Hanke, cond-mat/0511460.

[50] Y. Sidis, P. Bourges, C. Bernhard, C. Niedermayer, L.P. Regnault, N.H. Andersen, and B. Keimer, Phys. Rev. Lett. **86**, 4100 (2001).

[51] H. Mukuda, M. Abe, Y. Araki, Y. Kitaoka, K. Tokiwa, T. Watanabe, A. Iyo, H. Kito, and Y. Tanaka, Phys. Rev. Lett. **96**, 087001 (2006).

[52] O.P. Sushkov and V.N. Kotov, Phys. Rev. B **70**, 024503 (2004); V.N. Kotov and O.P. Sushkov, Phys. Rev. B **70**, 195105 (2004).

[53] E. Cappelluti and R. Zeyher, Phys. Rev. B **59**, 6475 (1999).

[54] S. Chakravarty, R.B. Laughlin, D.K. Morr, and C. Nayak, Phys. Rev. B **63**, 094503 (2001).

[55] C. Honerkamp, M. Salmhofer, and T.M. Rice, Eur. Phys. J. B **27**, 127 (2002).

[56] R. Micnas, J. Ranninger, and S. Robaszkiewicz, Rev. Mod. Phys. **62**, 113 (1990).